Photon Transport in a Bose-Hubbard Chain of Superconducting Artificial Atoms

G. P. Fedorov,[1,2,3,*] S. V. Remizov,[4,5] D. S. Shapiro,[4,5] W. V. Pogosov,[4,6] E. Egorova,[1,2,3] I. Tsitsilin,[1,2,3] M. Andronik,[7] A. A. Dobronosova,[7,4] I. A. Rodionov,[7,4] O. V. Astafiev,[8,1,9,10] and A. V. Ustinov[2,11,3]

[1]*Moscow Institute of Physics and Technology, 141701 Dolgoprundiy, Russia*
[2]*Russian Quantum Center, National University of Science and Technology MISIS, 119049 Moscow, Russia*
[3]*National University of Science and Technology MISIS, 119049 Moscow, Russia*
[4]*Dukhov Automatics Research Institute, (VNIIA), 127055 Moscow, Russia*
[5]*Kotel'nikov Institute of Radio Engineering and Electronics, Russian Academy of Sciences, 125009 Moscow, Russia*
[6]*Institute for Theoretical and Applied Electrodynamics, Russian Academy of Sciences, 125412 Moscow, Russia*
[7]*FMN Laboratory, Bauman Moscow State Technical University, 105005 Moscow, Russia*
[8]*Skolkovo Institute of Science and Technology, 121205 Moscow, Russia*
[9]*Physics Department, Royal Holloway, University of London, Egham, Surrey TW20 0EX, United Kingdom*
[10]*National Physical Laboratory, Teddington TW11 0LW, United Kingdom*
[11]*Physics Institute and Institute for Quantum Materials and Technologies, Karlsruhe Institute of Technology, 76131 Karlsruhe, Germany*

(Received 15 December 2020; accepted 16 March 2021; published 7 May 2021)

We demonstrate nonequilibrium steady-state photon transport through a chain of five coupled artificial atoms simulating the driven-dissipative Bose-Hubbard model. Using transmission spectroscopy, we show that the system retains many-particle coherence despite being coupled strongly to two open spaces. We find that cross-Kerr interaction between system states allows high-contrast spectroscopic visualization of the emergent energy bands. For vanishing disorder, we observe the transition of the system from the linear to nonlinear regime of photon blockade in excellent agreement with the input-output theory. Finally, we show how controllable disorder introduced to the system suppresses nonlocal photon transmission. We argue that proposed architecture may be applied to analog simulation of many-body Floquet dynamics with even larger arrays of artificial atoms paving an alternative way towards quantum supremacy.

DOI: 10.1103/PhysRevLett.126.180503

There has been increased effort over recent years in on-chip simulation of various solid state and quantum optical models using superconducting circuits [1]. The Bose-Hubbard (B-H) model is now particularly well covered as it can be straightforwardly mapped onto arrays of coupled transmon qubits [2,3]. The pioneering work [4] had demonstrated this for a three-site linear lattice, and subsequent experiments were focused on simulating dynamics with engineered dissipation [5], investigating the many-body localization phase transitions [6–8], and correlated quantum walks [9,10]. As numerous theoretical studies propose a new research direction involving controllable light-matter interaction and Floquet engineering to study periodically driven Hamiltonians and their nonequilibrium dynamics [11–15], it is tempting to use transmon chains to simulate the driven-dissipative Bose-Hubbard model. The subject is particularly promising since a recent study has shown that driven systems may open new way for demonstration of quantum supremacy [16].

In this Letter, we present a proof-of-principle device that models nonequilibrium steady-state boson transport through a Bose-Hubbard chain [17–20] using a linear array of five transmons strongly coupled to semi-infinite waveguides at its edges. While dominating over other loss channels, this strong coupling is still small compared to the interaction between the transmons. As the coherence between sites is not destroyed by the interaction with the continuum of electromagnetic modes, the suggested architecture is usable for many-body Floquet simulations with the ability to capture emitted quantum light. Moreover, the device complements prior theoretical research on the transmission spectroscopy of quantum metamaterials [21–26] with direct experimental data. We also expect that similar systems may be used to test the accuracy of methods of contraction of the Hilbert space such as the matrix product states or tensor networks in general [2,18,27].

The layout of the chip is shown in Fig. 1(a). We use five capacitively coupled Xmon qubits tunable via individual flux lines [5,28]. Strong coupling to the open spaces is attained via large interdigitated capacitors at the input and output waveguides and allows us to measure the microwave transmission through the system. In Fig. 1(b), we illustrate the physical model simulated by the device; the corresponding Hamiltonian including the coherent drive is

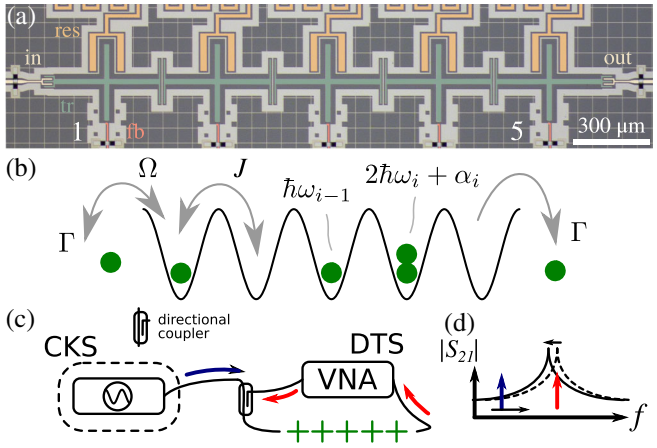

FIG. 1. (a) Optical image of the device (false colored). Input and output waveguides (beige) are strongly coupled to the edge transmons (green). All transmons can be dispersively read out via auxiliary resonators (orange) and tuned via flux bias lines (red). (b) Model of the device—a B-H lattice with five sites. Bosons are inserted from the left by the drive of strength Ω and leak predominantly from the sides at rate Γ. The energy of an ith localized boson is $\hbar\omega_i$, adding another boson to the same site costs $\hbar\alpha_i < 0$. Bosons can tunnel between sites at rate J. (c) Schematic of the measurement setup: the direct transmission spectroscopy (DTS) is done using the vector network analyzer which measures the complex transmission S_{21}. The cross-Kerr spectroscopy (CKS) requires an additional microwave source connected through a directional coupler. (d) CKS is done by sweeping the source frequency (blue arrow) while monitor ing the transmission at a certain resonance peak via the VNA (red arrow).

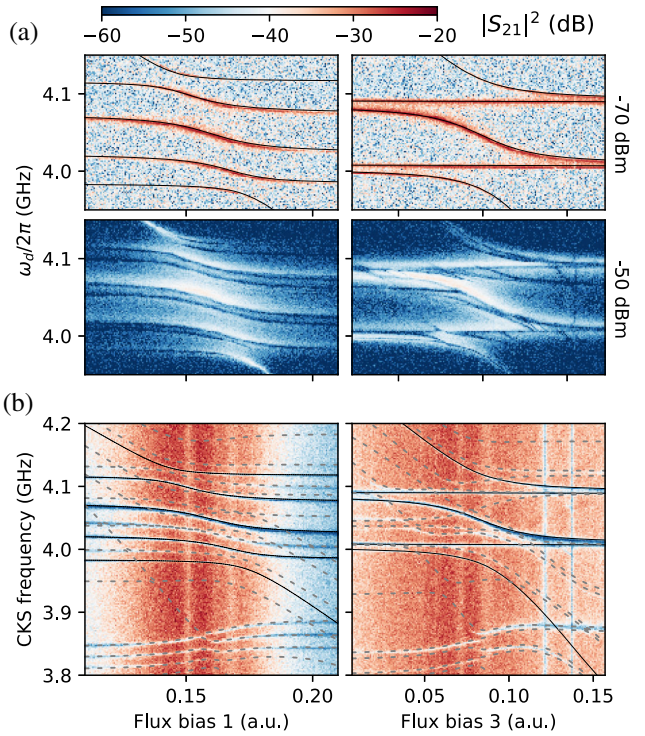

FIG. 2. (a) DTS of the chain. S_{21} includes the attenuation and amplification in the measurement chain, VNA output power is shown on the right. In the top row, black lines are the fit of the lowest five transitions of Eq. (1) for $J/2\pi = 41$ MHz, $\omega_i/2\pi \approx 4.05$ GHz. (b) CKS via the third mode showing the emergent band structure of the system. Dashed lines fit the frequencies of the purely quantum transitions.

$$\hat{H}/\hbar = \sum_{i=1}^{5}\left[(\omega_i - \omega_d)\hat{b}_i^\dagger\hat{b}_i + \frac{1}{2}\alpha_i\hat{b}_i^\dagger\hat{b}_i(\hat{b}_i^\dagger\hat{b}_i - 1)\right] + J\sum_{i=1}^{4}[\hat{b}_{i+1}^\dagger\hat{b}_i + \hat{b}_{i+1}\hat{b}_i^\dagger] + \frac{\Omega}{2}(\hat{b}_1^\dagger + \hat{b}_1), \quad (1)$$

where $\hat{b}_i$, $\hbar\omega_i$, and $\hbar\alpha_i$ are, respectively, the lowering operator, single-boson energy, on-site interaction for the ith site; J is the site-site tunneling rate, and ω_d is the drive frequency [3,29,30]. The dissipation being essential to the dynamics is included in the corresponding Liouville equation using Lindbladian superoperators with the collapse operators describing the relaxation and the pure dephasing for each site at rates γ_i and $\gamma_\phi^{(i)}$, respectively (see Supplemental Material [31] for the explicit formulation). Strong coupling to the edge lines implies $\gamma_1 \approx \gamma_5 \approx \Gamma$ to be the dominating source of decoherence. If $\omega_i = \omega$, $\alpha_i = \alpha$, the standard B-H Hamiltonian is restored.

In Fig. 1(c) we show schematically the experimental setup. We measure the transmission $S_{21}(\omega_d)$ through the chain using a vector network analyzer (direct transmission spectroscopy, DTS) and optionally use an additional microwave source to perform the cross-Kerr spectroscopy (CKS) of the system; in both cases, with the continuous microwave excitation we study the steady-state properties of the device. To obtain theoretical predictions for the S_{21} in DTS, one can use the input-output formalism [32–34]. Since we irradiate the system coherently, we assume that the input field mode amplitude is related to the coherent drive strength Ω in the driving operator $\hbar\Omega\hat{b}_1\cos\omega t$ via $\sqrt{\gamma_1}\langle\hat{b}_{\rm in}^\dagger\rangle \approx i\Omega/2$, which follows from the quantum Langevin equations [35]. Similarly, the output field operator $\hat{b}_{\rm out}^\dagger \approx \sqrt{\gamma_5}\hat{b}_5^\dagger$. From this, we obtain $S_{21} = \langle\hat{b}_{\rm out}^\dagger\rangle/\langle\hat{b}_{\rm in}^\dagger\rangle = 2\Gamma\cdot{\rm Tr}[\hat{\rho}_{ss}\hat{b}_5^\dagger]/i\Omega$, where $\hat{\rho}_{ss}$ is the steady-state density matrix. Physically, this expression means that the signal transmission is possible if the rightmost transmon becomes non-locally excited while the leftmost is subject to radiation. Indeed, from the linearized Langevin equations [31,36] ($\Omega \ll \Gamma$) follows that at the degeneracy point ($\omega_i = \omega$) five transmission peaks detuned $0, \pm J, \pm\sqrt{3}J$ from ω should appear due to the interaction, corresponding to the classical normal mode frequencies. The widths of the central, next-to-central, and edge peaks are $2\Gamma/3$, $\Gamma/2$, and $\Gamma/6$, respectively, and add up to 2Γ [31]. In the quantum-mechanical limit, these resonances should remain in the spectrum due to the correspondence

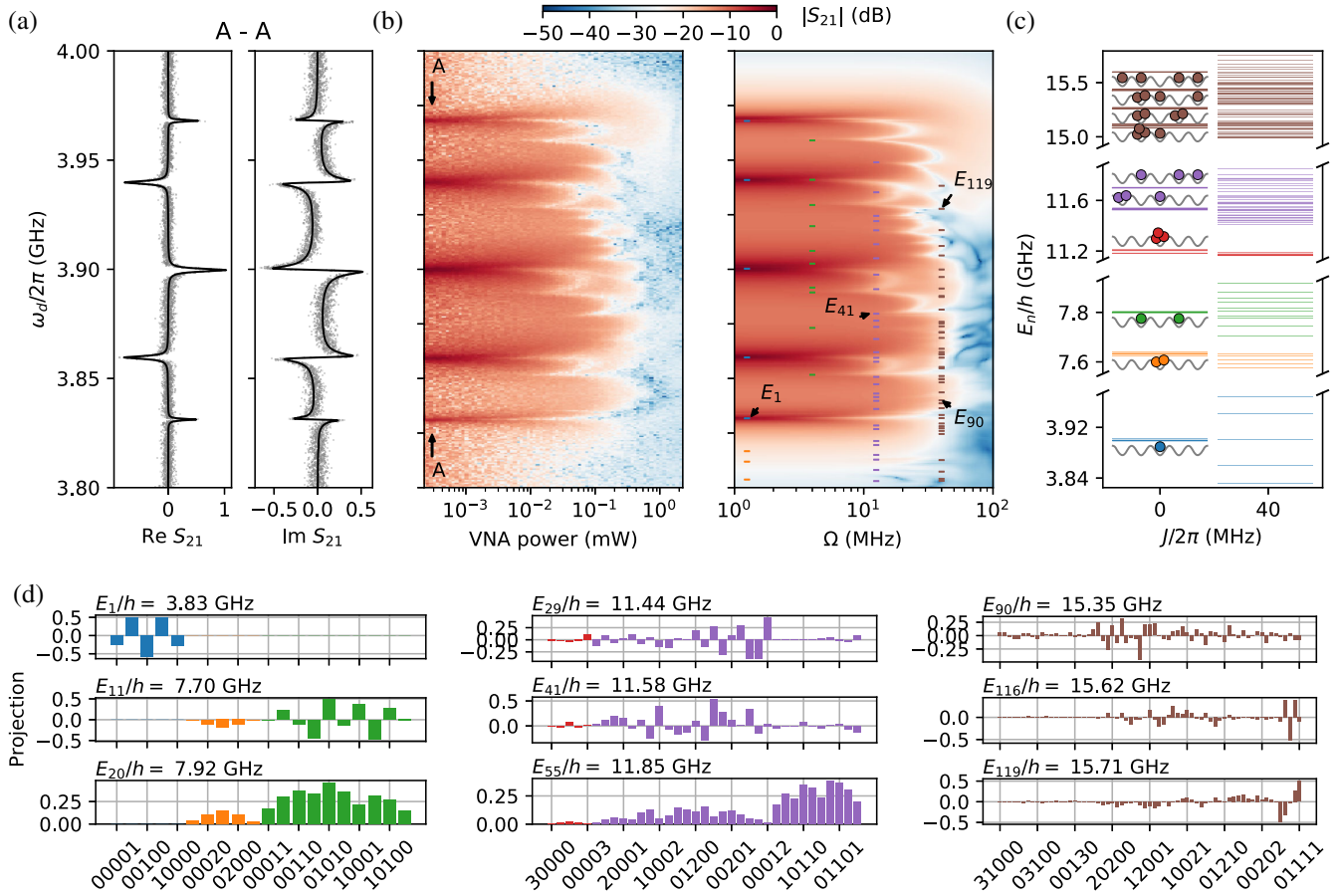

FIG. 3. (a) The analytical solution for the S_{21} in the linear regime (smooth curves) fitted to the low power data (clouds), normalized. (b) Experimental and simulated $|S_{21}|$ for various driving powers. Driving power is calibrated to match the Rabi frequency Ω of the simulation. Dashes show the corresponding multiphoton transition frequencies calculated using the eigenlevels from (c). (c) The energy level structure of the model with and without interaction using the parameters extracted from the fits; three excitations per site are included, and up to four excitations total; E_n is the energy of the nth eigenstate, $E_0 = 0$. (d) Relevant many-body eigenstates projected onto the unperturbed basis [colors as in (c)]. The inherent randomness in the decompositions of the high-energy states conditions the random structure of the energy levels.

principle; however, new lines caused by purely quantum-mechanical processes are expected to appear in the nonlinear regime.

The results of the DTS are shown in Fig. 2(a). To unveil the structure of the eigenmodes and to extract ω_i and J, we bias one of the transmons across the degeneracy point while keeping the others at around 4.05 GHz. In the left column, the first transmon is swept, and in the right, the middle one. The first transmon interacts with all collective states, and the third only with the odd ones; this behavior is expected from the Hamiltonian. We find the tunnelling rate $J/2\pi$ to be around 41 MHz from the numerical fit. When the incident power is increased, the resonances are subject to photon blockade [37] and behave similarly to what is observed for single superconducting qubits [36]. In the bottom row of Fig. 2(a), we notice spectral manifestations of the many-body states of the system which do not have classical counterparts. We thus call the power-dependent behavior shown in Fig. 2(a) a classical-quantum transition.

The remaining parameters α_i of Eq. (1) can be extracted via the CKS. In Fig. 2(b) we have done it using the same two configurations of the transmon frequencies as in Fig. 2(a) and performed another numerical fit (solid and dashed lines). The readout tone was aimed at the third mode, so the observed spectral frequencies should be corrected by adding its frequency for each bias voltage. The dashed lines show the emergent bands of the two-photon subspace: the many-body states with two excitations at different sites are near 4.05 GHz and "doublons" [38] are located around 3.85 GHz. The B-H eigenstates with doubly populated sites have lower energy due to the attractive interactions; the disorder in the extracted values of $\alpha_i/2\pi$ of approximately $[-188, -178, -178, -178, -188]$ MHz is around 5% and is caused by the uncompensated capacitance to the transmission lines.

To further study the energy structure and nonequilibrium dynamics of the system during the classical-quantum transition, we use a direct transmission experiment with fixed degenerate configuration of the transmon frequencies $\omega_i/2\pi = 3.9$ GHz. Using a fitting procedure similar to Fig. 2, we evaluate $\omega_i/2\pi$ to [3.898, 3.898, 3.9, 3.901, 3.901] GHz, where deviations from the target value come from the flux cross-talk. In the linear regime, we estimate the coupling to the transmission lines and internal dissipation from the fit of the complex transmission coefficient predicted by the linear model which is shown in Fig. 3(a). Using these data, we also estimate the transmission amplitude through the attenuation and amplification chain and find that the third mode has nearly unity transmission. This is expected as it interacts only with a single "bulk" transmon [see Fig. 2(a)] and thus has the least internal dissipation. Since in the linear model it is impossible to discern pure dephasing and internal dissipation, the relaxation rates from the fit are larger than true values: we estimate γ_i to be $[16, 6, 0.1, 3, 16]$ μs^{-1}; the rates γ_1 and γ_5 are in good agreement with the value calculated from the simulated edge capacitances of 8 fF and justify the assumption of dominating Γ.

Figure 3(b) shows how the transmission spectrum changes throughout the transition. The normal mode peaks gradually saturate due to the photon blockade and multiple new dips appear caused by reflective multiphoton transitions to the many-body eigenstates [18,25,30]. The experimental data agree very well with the numerical steady-state simulation in *qutip* [39,40] of the five-site Bose-Hubbard model with the parameters extracted earlier and three bosons per site at max; full simulation of 253×253 density matrix takes approximately a week on a 138 core cluster for the shown 300×300 heat map. The selection rules of the system do not allow all possible multiphoton lines, but one can clearly discern an increase of the density of states and their randomness with increasing band number. It can be connected to the classical chaoticity of the system if the distribution of the level spacings corresponds to the Gaussian orthogonal ensemble [41–44]. The frequencies of transitions up to four photon are shown with colored dashes and can be identified with the energy bands shown in Fig. 3(c) calculated using the fitted parameters of the model Eq. (1). The statistics of the calculated nearest-neighbor level spacings resembles the Wigner-Dyson distribution for the experimentally determined parameters, but is rather Poissonian for the ideal parameters which probably means that the system size is too low to obtain the correct histogram. To show how delocalized are the eigenstates $|n\rangle$ reachable in our device (n is counted excluding the states with more than three excitations per site), in Fig. 3(d) we project several of them onto the noninteracting basis. State $|1\rangle$ has the structure identical to the classical symmetric low-frequency eigenmode. States $|11\rangle$ and $|20\rangle$ are at the edges of the two-photon subspace

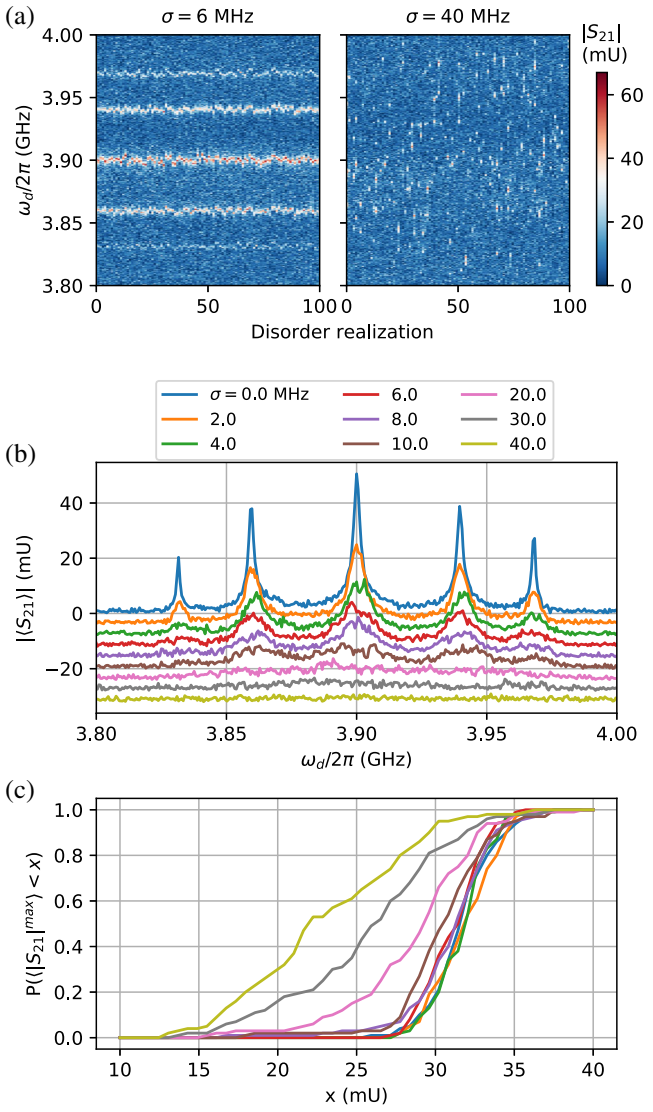

FIG. 4. (a) Raw transmission data for $\sigma = 6$, 40 MHz and 100 realizations of disorder; absolute value of the transmission is shown with color. (b) Localization and disappearance of transmission with increasing disorder. Each curve shows the absolute value of the averaged transmission over the Gaussian disorder realizations with a certain standard deviation σ shown in the legend. Each next curve is offset downwards for better visibility. (c) Probability distributions of the brightest peak prominence $\langle |S_{21}|^{\max} \rangle$ (see text) observed in the disorder realizations for the σ values from (b).

and form much larger superpositions. One can note the unfolding randomness in the decomposition coefficients, which becomes more and more pronounced for higher energies: no symmetries or even any kind of structure can be found in the higher eigenstates except for the holelike four-excitation subspace dual to the single-photon one (see $|116\rangle$, $|119\rangle$).

It is known that the Poissoinian statistics is usually a property of the disordered Bose-Hubbard model exhibiting localization [6,9,10]. To check how the localization

changes the transport properties, we introduce controllable disorder into the transmon frequencies near the degeneracy point in an experiment similar to what was done before numerically [2]: a certain common frequency variance σ is chosen, then the random frequency $\omega + \delta\omega$ is assigned to each transmon where $\delta\omega \in \mathbb{N}(0, 2\pi\sigma)$ and $\omega/2\pi = 3.9\,\mathrm{GHz}$. Then the transmission is recorded, and the full process is repeated 100 times. In Fig. 4(a) we show two examples of the raw transmission data for $\sigma = 6$, 40 MHz. As one can see, for the smaller standard deviation of the target frequencies, the eigenmodes stay relatively unchanged while for the larger the initial structure is completely lost. The averaged curves for several values of σ are shown in Fig. 4(b). One can see that when the noise in the transmon frequencies reaches the coupling strength $J/2\pi$, the averaged transmission vanishes. This means that the localization is revealed in the transport properties when the excitation of the first qubit on average does not reach the last qubit. This fact reminds us of the superconductor-insulator transition [45] to describe which was the initial purpose of the Bose-Hubbard model. As the transmission vanishes only on average and some peaks occasionally remain even for the largest σ, in Fig. 4(c) we also study the distribution of the brightest peak prominences (taken as the mean of 10 points around the maximum) seen over the disorder realizations and show that it also changes qualitatively when $\sigma \approx J/2\pi$.

In conclusion, we have shown how quantum photon transport occurs through a Bose-Hubbard chain simulated by transmon artificial atoms. We have demonstrated that the behavior of the single-photon subspace of the system does not deviate from the classical normal mode theory which is expected from the correspondence principle [46]. However, an increase of the incident photon flux beyond the dissipation rate reveals the quantum nature of the system through the photon blockade and multiphoton transitions to composite many-body states. The classical theory then fails, and one can only resort to numerical solution of the master equation to find the non-equilibrium steady state, which shows excellent agreement with the data. Finally, we have shown how controllable disorder affects the photon transport: we find that the transmission averaged over disorder realizations ceases when the standard deviation of the transmon frequencies reaches the interaction strength.

We gratefully acknowledge valuable discussions with I. Besedin, S. Flach, A. Poddubny, and A. Bychek. We thank D. Yakovlev and A. Sokolova for their help in preliminary experiments. The investigation was conducted with the support of Russian Science Foundation, Grants No. 21-42-00025 (measurement and data analysis) and 16-12-00095 (numerical modeling). Devices were fabricated at the BMSTU Nanofabrication Facility (Functional Micro/Nanosystems, FMNS REC, ID 74300). We also acknowledge support from the Ministry of Education and Science of the Russian Federation in the framework of the Increased Competitiveness Program of the National University of Science and Technology MISIS (Contract No. K2-2020-022).

*gleb.fedorov@phystech.edu

[1] M. Kjaergaard, M. E. Schwartz, J. Braumüller, P. Krantz, J. I.-J. Wang, S. Gustavsson, and W. D. Oliver, Annu. Rev. Condens. Matter Phys. **11**, 369 (2020).
[2] T. Orell, A. A. Michailidis, M. Serbyn, and M. Silveri, Phys. Rev. B **100**, 134504 (2019).
[3] Y. Yanay, J. Braumüller, S. Gustavsson, W. D. Oliver, and C. Tahan, npj Quantum Inf. **6**, 58 (2020).
[4] S. Hacohen-Gourgy, V. V. Ramasesh, C. De Grandi, I. Siddiqi, and S. M. Girvin, Phys. Rev. Lett. **115**, 240501 (2015).
[5] R. Ma, B. Saxberg, C. Owens, N. Leung, Y. Lu, J. Simon, and D. I. Schuster, Nature (London) **566**, 51 (2019).
[6] P. Roushan, C. Neill, J. Tangpanitanon, V. Bastidas, A. Megrant, R. Barends, Y. Chen, Z. Chen, B. Chiaro, A. Dunsworth *et al.*, Science **358**, 1175 (2017).
[7] B. Chiaro, C. Neill, A. Bohrdt, M. Filippone, F. Arute, K. Arya, R. Babbush, D. Bacon, J. Bardin, R. Barends *et al.*, arXiv:1910.06024.
[8] M. C. Collodo, A. Potočnik, S. Gasparinetti, J.-C. Besse, M. Pechal, M. Sameti, M. J. Hartmann, A. Wallraff, and C. Eichler, Phys. Rev. Lett. **122**, 183601 (2019).
[9] Z. Yan, Y. R. Zhang, M. Gong, Y. Wu, Y. Zheng, S. Li, C. Wang, F. Liang, J. Lin, Y. Xu, C. Guo, L. Sun, C. Z. Peng, K. Xia, H. Deng, H. Rong, J. Q. You, F. Nori, H. Fan, X. Zhu, and J. W. Pan, Science **364**, 753 (2019).
[10] Y. Ye, Z. Y. Ge, Y. Wu, S. Wang, M. Gong, Y. R. Zhang, Q. Zhu, R. Yang, S. Li, F. Liang, J. Lin, Y. Xu, C. Guo, L. Sun, C. Cheng, N. Ma, Z. Y. Meng, H. Deng, H. Rong, C. Y. Lu, C. Z. Peng, H. Fan, X. Zhu, and J. W. Pan, Phys. Rev. Lett. **123**, 050502 (2019).
[11] N. Goldman and J. Dalibard, Phys. Rev. X **4**, 031027 (2014).
[12] J. Eisert, M. Friesdorf, and C. Gogolin, Nat. Phys. **11**, 124 (2015).
[13] S. Zippilli, M. Grajcar, E. Il'Ichev, and F. Illuminati, Phys. Rev. A **91**, 022315 (2015).
[14] O. Kyriienko and A. S. Sørensen, Phys. Rev. Applied **9**, 064029 (2018).
[15] S. Franca, F. Hassler, and I. C. Fulga, arXiv:2001.08217.
[16] J. Tangpanitanon, S. Thanasilp, M.-A. Lemonde, and D. G. Angelakis, arXiv:1906.03860.
[17] M. Leib and M. J. Hartmann, New J. Phys. **12**, 093031 (2010).
[18] A. Biella, L. Mazza, I. Carusotto, D. Rossini, and R. Fazio, Phys. Rev. A **91**, 053815 (2015).
[19] T. Mertz, I. Vasić, M. J. Hartmann, and W. Hofstetter, Phys. Rev. A **94**, 013809 (2016).
[20] A. A. Bychek, P. S. Muraev, D. N. Maksimov, and A. R. Kolovsky, Phys. Rev. E **101**, 012208 (2020).
[21] A. M. Zagoskin, D. Felbacq, and E. Rousseau, Eur. Phys. J. Quantum Technol. **3**, 2 (2016).

[22] O. Viehmann, J. von Delft, and F. Marquardt, Phys. Rev. Lett. **110**, 030601 (2013).
[23] Y. S. Greenberg and A. A. Shtygashev, Phys. Rev. A **92**, 063835 (2015).
[24] M. V. Fistul and M. A. Iontsev, Phys. Rev. A **100**, 023844 (2019).
[25] D. Roberts and A. A. Clerk, Phys. Rev. X **10**, 021022 (2020).
[26] T. Tiwari, D. Roy, and R. Singh, arXiv:2010.14935.
[27] A. Di Paolo, T. E. Baker, A. Foley, D. Sénéchal, and A. Blais, arXiv:1912.01018.
[28] X. Li, Y. Ma, J. Han, T. Chen, Y. Xu, W. Cai, H. Wang, Y. P. Song, Z.-Y. Xue, Z.-q. Yin *et al.*, Phys. Rev. Applied **10**, 054009 (2018).
[29] E. Egorova, G. Fedorov, I. Tsitsilin, I. Besedin, and A. Ustinov, AIP Conf. Proc. **2241**, 020013 (2020).
[30] G. P. Fedorov, V. B. Yursa, A. E. Efimov, K. I. Shiianov, A. Y. Dmitriev, I. A. Rodionov, A. A. Dobronosova, D. O. Moskalev, A. A. Pishchimova, E. I. Malevannaya, and O. V. Astafiev, Phys. Rev. A **102**, 013707 (2020).
[31] See Supplemental Material at http://link.aps.org/supplemental/10.1103/PhysRevLett.126.180503 for full master equation, linear solution for the transmission, two-qutrit and five-qubit perturbative solutions, sample fabrication details.
[32] B. Yurke and J. S. Denker, Phys. Rev. A **29**, 1419 (1984).
[33] M. J. Collett and C. W. Gardiner, Phys. Rev. A **30**, 1386 (1984).
[34] C. W. Gardiner and M. J. Collett, Phys. Rev. A **31**, 3761 (1985).
[35] M. Mirhosseini, E. Kim, X. Zhang, A. Sipahigil, P. B. Dieterle, A. J. Keller, A. Asenjo-Garcia, D. E. Chang, and O. Painter, Nature (London) **569**, 692 (2019).
[36] O. Astafiev, A. M. Zagoskin, A. Abdumalikov, Y. A. Pashkin, T. Yamamoto, K. Inomata, Y. Nakamura, and J. S. Tsai, Science **327**, 840 (2010).
[37] K. M. Birnbaum, A. Boca, R. Miller, A. D. Boozer, T. E. Northup, and H. J. Kimble, Nature (London) **436**, 87 (2005).
[38] M. A. Gorlach, M. Di Liberto, A. Recati, I. Carusotto, A. N. Poddubny, and C. Menotti, Phys. Rev. A **98**, 063625 (2018).
[39] J. Johansson, P. Nation, and F. Nori, Comput. Phys. Commun. **183**, 1760 (2012).
[40] J. Johansson, P. Nation, and F. Nori, Comput. Phys. Commun. **184**, 1234 (2013).
[41] O. Bohigas, M.-J. Giannoni, and C. Schmit, Phys. Rev. Lett. **52**, 1 (1984).
[42] T. Zimmermann, H.-D. Meyer, H. Köppel, and L. S. Cederbaum, Phys. Rev. A **33**, 4334 (1986).
[43] A. R. Kolovsky and A. Buchleitner, Europhys. Lett. **68**, 632 (2004).
[44] G. Livan, M. Novaes, and P. Vivo, *Introduction to Random Matrices: Theory and Practice* (Springer, New York, 2018), Vol. 26.
[45] C. Bruder, R. Fazio, and G. Schön, Phys. Rev. B **47**, 342 (1993).
[46] D. Park, *Classical Dynamics and Its Quantum Analogues* (Springer Science & Business Media, New York, 2012).